CONF-78-128-E
Pg 154
RECEIVED
JAN 5 1979
DIRECTORS OFFICE
FERMILAB

Cluster "Creation" in 147 GeV/c $\pi^- p$ Interactions

Irwin A. Pless

Massachusetts Institute of Technology

Cambridge, Massachusetts 02139 USA

Invited Talk

submitted to

IX International Symposium on High Energy Multiparticle Dynamics

Tabor, Czechoslovakia

July 2-7, 1978

I. Introduction

One of the features of multiparticle production at high energies is a leading particle effect, while another feature is the appearance of short-range order. A third feature, well known even at low energies, is the limited transverse momentum distribution of the produced particles.

Examination of the available data has led to the concept of clusters, i. e., the creation of particles in small, correlated groups. When "seen" at high transverse momentum, these groups are called jets. However, these clusters are not self-evident in the data at current energies. Hence, physicists have examined the data and in a sense "created" these clusters. This paper will describe two ways of "creating" clusters and their possible physical implications.

The first is a zone graph technique suggested by Kryzwicki and Weingarten[1] which "picks" out clusters in rapidity space. The second method is a nearest neighbor technique, first exploited by Ludlam[2], which effectively operates in invariant mass space. Both these techniques define clusters in different ways, but each of them has arbitrary aspects which are chosen to give the best results.

The zone graph technique results in a model which has two leading clusters and a central fireball. Figure (1) describes this picture.

The nearest neighbor technique views the interaction as creating a number of small clusters, each of which has its individual properties. Figure (2) displays this viewpoint.

II. Data Acquisition

The data I will describe comes from experiments using the Fermilab hybrid spectrometer. Figure (3) shows that layout. The principle component of the spectrometer is the 30" hydrogen bubble chamber. The upstream Čerenkov counter and proportional wire chamber system identifies the incoming beam particles and

the downstream proportional wire chambers measure the trajectories of secondary particles from the interactions in the bubble chamber.

III. Modified Zone Graph Technique and the Leading Charge Model

The universities associated with this work are shown in fig. (4). The space this work concerns itself with is rapidity space, $Y = \frac{1}{2} \ln\left(\frac{E + P_L}{E - P_L}\right)$. Figure (5) shows a typical 10-prong event. It also describes the construction of the zones associated with this event. As the example shows, one ends up with zones that are really determined by the change in charge and not determined by any "distance" in rapidity space. The "creation" of clusters from this data is done in the following model. We assume that there are two leading clusters in every interaction and that these leading clusters have the same charge as the original target and beam that created them. Hence, we define beam end zone as the group of particles (usually 1 or 3) with the highest rapidity that have the charge of the beam. We also define a target end zone as the group of particles (again, usually 1 or 3) with the lowest rapidity that have the charge of the target. We define a beam cluster of an event as the particles in the beam end zone plus any minus-plus pion pairs within 1.0 units of rapidity of the beam end zone. We define a target cluster of an event as the particles in the target end zone plus any minus-plus pion pairs within 1.3 units of rapidity of the target end zone. About 80% of both beam and target end zones contain only one particle, while an additional 10% contain three particles. Therefore, in somewhat over 90 percent of the events, the fastest one or three particles carry the charge of the beam,and in somewhat over 90 percent of the events, the fastest one or three particles in the target direction carry the charge of the target. Hence, for the great majority of the events, it is simple to define the leading clusters.

We therefore propose a leading charge model (LCM) which consists of two leading clusters and a central cluster. The central cluster is defined to be all the particles not in either leading cluster.

The properties of this model are: (1) the central cluster has random distribution in charge, and (2) the transverse momentum and longitudinal momentum distributions of the central cluster are similar. We therefore call the central cluster a fireball.

To show that the central cluster indeed has a random charge distribution, we first look at the charge asymmetry for all the data and for the central cluster. We define the charge asymmetry A(y) to be:

$$A(y) = \frac{\left.\frac{d\sigma}{dy}\right|_{+} - \left.\frac{d\sigma}{dy}\right|_{-}}{\left.\frac{d\sigma}{dy}\right|_{+} + \left.\frac{d\sigma}{dy}\right|_{-}}$$

Figure (6) is a plot of A(y) for all the data and the central fireball. As is displayed, the data for all the events falls smoothly through zero at $y = 0$ with no hint of a zero asymmetry plateau. On the other hand, the data for the central fireball exhibits a clear zero asymmetry plateau, around $y = 0$. This is one indication that the selected fireball particles indeed have a random charge distribution.

The details of a further test made to determine whether or not the central fireball indeed has random charge distribution is shown in fig. (7). In this test, which simulates closely the LCM discussed earlier, we identify the two leading clusters in each event and then in a random way reassign the charges of the central cluster or fireball. In this process, we, of course, conserve overall charge. We now have a new sample of events which has been constructed so as to ensure that the central cluster has random charge distribution. We can now compare detailed distributions of this new, leading charge model (LCM) sample with the original data.

The first quantity we compare is the charge transfer variable U, first defined by Chou and Yang[3]:

$$U = \frac{1}{2}(Q_F - Q_B)_{final} - \frac{1}{2}(Q_F - Q_B)_{initial}$$

where Q_F (Q_B) is the total charge in the forward (backward) hemisphere. Figure 8(a) displays this distribution.

Notice that the LCM sample, constructed from the data, reproduces the data quite precisely. This is another indication that the charge in the "fireball" is randomly distributed. The dotted line in fig. 8(a) is the distribution you generate if you randomize all the charges in an event (Random Charge Model - RCM). Note that this model, as expected, does not match the data at all.

Another test of randomness of charge of the fireball is to compare the zone multiplicity distribution of the data with the LCM sample. Figure 8(b) displays this comparison. Again, the LCM sample follows the data quite accurately. We also compare the data with the sample of events with all the charges in the event randomized (RCM). As seen before, this random charge model sample does not match the data.

The zone distribution comparison can be made more detailed by examining the semi-inclusive zone distributions. Figure (9) displays these distributions. Here we see in detail how the LCM sample tracks the data. The RCM sample consistently fails to match the data.

We have made many other tests to see if the data is consistent with the hypothesis that the selected fireball particles indeed are randomly distributed in charge and all tests are affirmative.

Having established that our fireball is randomly distributed in charge, let us turn our attention to the momentum distribution of the particles in the fireball. Van Hove [4] has defined a cluster as an aggregate of final particles such that in the rest system of this aggregate, the longitudinal and the transverse momenta of the particles are similar. In fig. 10(a), the center-of-mass longitudinal and transverse momenta of all final particles in $\pi^- p$ interactions are compared. As is well known,

the effect of limited transverse momenta exhibits itself in this plot; that is, the particles contain larger amounts of longitudinal momenta than transverse momenta. In fig. 10(b), we see a comparison of the longitudinal and transverse momenta of charged particles in the central fireball. The two components follow very similar distributions. These data satisfy Van Hove's definition of what constitutes a cluster. Of immediate interest is the angular distribution of the particles in the fireball. Figure 11 shows this distribution as a function of the momentum of the particles. As can be seen for momenta less than 600 MeV/c, the distributions are quite isotropic with only the fast particles ($p > 600$ MeV/c) being strongly anisotropic. These fast particles represent about 25% of the total number that make up the fireball. This nearly isotropic behavior and the randomness of the charge distribution account for our designating these central cluster particles a "fireball."

Figure 12 shows the multiplicity distribution of this central fireball. The average multiplicity of the fireball is about three while the average multiplicity per event is about seven. Various theories [5, 6, 7, 8, 9] predict that the relation between the multiplicity n of a fireball and the mass M of a fireball should be of the form

$$n = M^{b} \quad .$$

Figure 12(b) shows the plot of our data. The best fit is:

$$b = .64 \pm .03.$$

This is close to the 2/3 predicted by Feinberg [9] based on a modified Landau model.

Given a fireball, one can ask, "Does it have a Bose distribution in momentum and, if so, what is the characteristic temperature?" Figure 13 is our data and a fit to the momentum distribution of the form:

$$F(p) = \frac{A\,p^2}{e^{E/T}-1}$$

for $p < 800$ MeV/c. The fit gives $T = 131 \pm 2$ MeV. with a reasonable X^2.

What we have demonstrated is that by a simple and perhaps somewhat arbitrary procedure, it is possible to separate each event into three regions: a beam cluster, a target cluster, and a central fireball. This central fireball satisfies Van Hove's definition of a cluster; namely, the transverse and longitudinal momentum distributions are similar. It also has isotropic angular distribution and the charge distribution is random. The Bose temperature is 131 MeV. This picture satisfies some theoretical speculations; in particular, Pokorski and Van Hove[10] see an interaction as the target and beam passing through the interaction region with their identities conserved, producing two leading clusters, while the central region particles are produced by gluon interactions. Note that this clustering algorithm was based almost solely on charge configuration and almost not at all on any kinematic considerations. Namely, it required the fastest group of particles to have the same charge as either the beam or target, which created two clusters and all the rest was the third cluster. Kinematics played a relatively minor role.

IV. Nearest Neighbor Technique

Another technique for "creating" clusters essentially ignores charge altogether and basically depends on kinematics. The people associated with this are listed in fig. 14. In this approach, one looks for clustering in invariant mass space. One defines a metric, dij, between any two particles i and j with mass M_i and M_j in an event in the following way:

$$(dij)^2 = (M_{ij})^2 - (M_i + M_j)^2 .$$

M_{ij} is the invariant mass of the two particles.

The metric dij has the following properties:

(1) It is Lorentz invariant

(2) It is positive

(3) If the relative velocity between the two particles is zero, then dij = 0.

Having defined a metric, then for each event one can form the "minimal spanning tree" for that event. The minimal spanning tree is a set of distances connecting pairs of particles in the event which has the following properties:

1. There is a path from every particle to every other particle in the event.
2. The total path length is a minimum.

The distance from point to point along the tree is called an edge. Given this "spanning tree" the question that arises is can one detect clusters of particles in the geometry of the tree. Figure (15) is an example of a spanning tree. An obvious way to "create" clusters is to pick a threshold distance and cut all the edges greater than this threshold distance. This would create clusters whose mass would depend on this threshold distance. To avoid this choice of threshold distance, we have utilized the concept of nearest neighbor. The nearest neighbor to a particle is that particle which is the smallest distance away. We then cut all the edges we can so as to leave all nearest neighbors connected to each other by edges. In fig. 15 the only edge we can cut is the edge connecting particle (1) to particle (5). This partitions the event into two clusters where each particle is in the same cluster as its nearest neighbor. This technique will break up an event into the maximum number of clusters where each cluster, if it contains a particle, will contain its nearest neighbor. This algorithm does not adequately handle leading particles, hence, it is also necessary to break all edges which are longer than 1.3 GeV/c^2.

We have taken Monte Carlo data whose cluster structure we know and tested the above algorithm to see how well it reproduces the known cluster structure. We

assumed the reaction $\pi^- + p \rightarrow w_1 + w_2 + w_3 + w_4 + N$. Each w_i was allowed to decay into a π_i^+, π_i^-, and π_i^0.

This is a 13 body final state containing eight charged particles. A perfect algorithm would divide each event into four clusters where each cluster contained the correct $\pi_i^+ \pi_i^-$ pair.

We generated 1,000 events and the result of our test is shown in fig. (16). Of the 4,000 correct $\pi^+\pi^-$ pairs, 3,599 appear either in two-particle, four-particle, or six-particle clusters. Hence, our algorithm generally put the correct $\pi^+\pi^-$ pair into the same cluster; however, over half of the time it joined two or three clusters together. This positive result led us to try the algorithm on our 147 GeV/c $\pi^- p$ data. Figure 17 shows the cluster multiplicity distribution. The average cluster multiplicity is just over three. Figure 18 shows the cluster distribution as a function of event charge prong multiplicity. As can be seen, the number of clusters for each topology grows with increasing topology, but the multiplicity of each cluster tends to be independent of topology.

To check whether the clusters located have physical meaning, we looked at all two-cluster events where one cluster contained an identified proton. The cluster not containing the proton should be rich in ρ^0 mesons. Figure 19 shows the $\pi^+\pi^-$ invariant mass for those clusters. As expected, there is a ρ^0 shoulder. To test if the shoulder is real or not, we took the mass recoiling against the proton and had that mass decay randomly, assuming the number of π^0's in each event to be equal to one-half the number of charged pions in the recoiling mass. The solid curve is the Monte Carlo result. There is an excess of events in the ρ^0 region over that predicted by the Monte Carlo.

One can now take the created clusters and plot their transverse momentum distribution. We chose clusters where the maximum individual pion P_T was less than

1.5 GeV/c^2. Figure 20 plots the single pion P_T and the cluster P_T distributions. Note that the cluster P_T distribution extends beyond a P_T of 2.5 GeV/c even though there is an absolute cutoff of 1.5 GeV/c^2 on the individual pions. It is instructive to compare our cluster P_T distribution to the jet distribution of Bromberg et al. (11) which is done in fig. 21. Note that that figure is plotted in terms of an invariant cross section and our data tends to join in a reasonably smooth fashion with the data from Fermilab. While our cluster creation technique is somewhat arbitrary, it is important to note that our low P_T data joins onto the high P_T data in such a smooth fashion. The trigger logic used in the Fermilab experiment is different from our clustering algorithm but the two techniques seem to give consistent results. The conclusion one may draw is either that both experiments are detecting physical entities which manifest themselves independently of the technique used to locate them or any clustering algorithm will find the same P_T distributions in the data even though the clusters created have no physical significance.

We have generated events with a limited P_T distribution which have the same topological properties as the data. The generated events when run through our clustering program do not reproduce the data shown in fig. 21. We deduce from this that either our Monte Carlo is too naive or fig. 21 represents real dynamics.

V. Conclusion

In conclusion, we have presented two distinct techniques for generating clusters from our 147 GeV/c $\pi^- p$ data. The first yields a picture with three clusters: two leading clusters with properties of the beam and target, and a central cluster, a fireball with temperature of 130 MeV. The fireball is isotropic in charge, angular in distribution, and has similar transverse and longitudinal momentum distributions.

The second technique generates clusters that have a P_T distribution that extends beyond the individual pion P_T distribution and joins on smoothly with the high P_T jet structure found in the Fermilab experiments.

It may be that the true physical situation is a combination of both phenomena and each technique singles out one aspect of the dynamics. More data is required (and will be available next year) to explore this possibility.

One should note that all the work presented here refers only to charged particle structures. It is expected that the inclusion of neutral particles in the analysis will not alter any of the conclusions. However, when neutral pion data becomes available, it will be important to check this point.

Acknowledgments

We are indebted to Fermilab and its Neutrino Section for furnishing the film and the scanning and measuring teams at our institutions for the film analysis. This experiment could not have been performed without the excellent technical proficiencies of these groups.

References

(1) A. Kryzwicki and D. Weingarten, Phys. Lett. 50B, 265 (1974).

(2) T. Ludlam, "Structure in Momentum Space of Multiparticle Final States," Third Topical Meeting of Multidimensional Analysis of High Energy Data, Nijmegen, March 1978.

(3) T. T. Chou and C. N. Yang, Phys. Rev. D7, 1425 (1973).

(4) L. Van Hove, 3rd Hawaii Topical Conference on Particle Physics, August 1969.

(5) E. Fermi, Progr. Theor. Phys. 5, 570 (1950).

(6) L. D. Landau, Izv. Akad. Nauk SSSR 17, 51 (1953).

(7) I. Ya. Pomeranchuk, Kokl. Acad. Nauk SSSR 78, 889 (1951).

(8) F. Cooper, C. Frye, and E. Schonberg, Phys. Rev. D11, 192 (1975).

(9) E. L. Feinberg, Soviet Physics Uspekhi 14, 455 (1972).

(10) S. Pokorski and L. Van Hove, Acta Phys. Pol. B5, 229 (1974).

(11) Bromberg et al., Phys. Rev. Lett. 38, 1447 (1977).

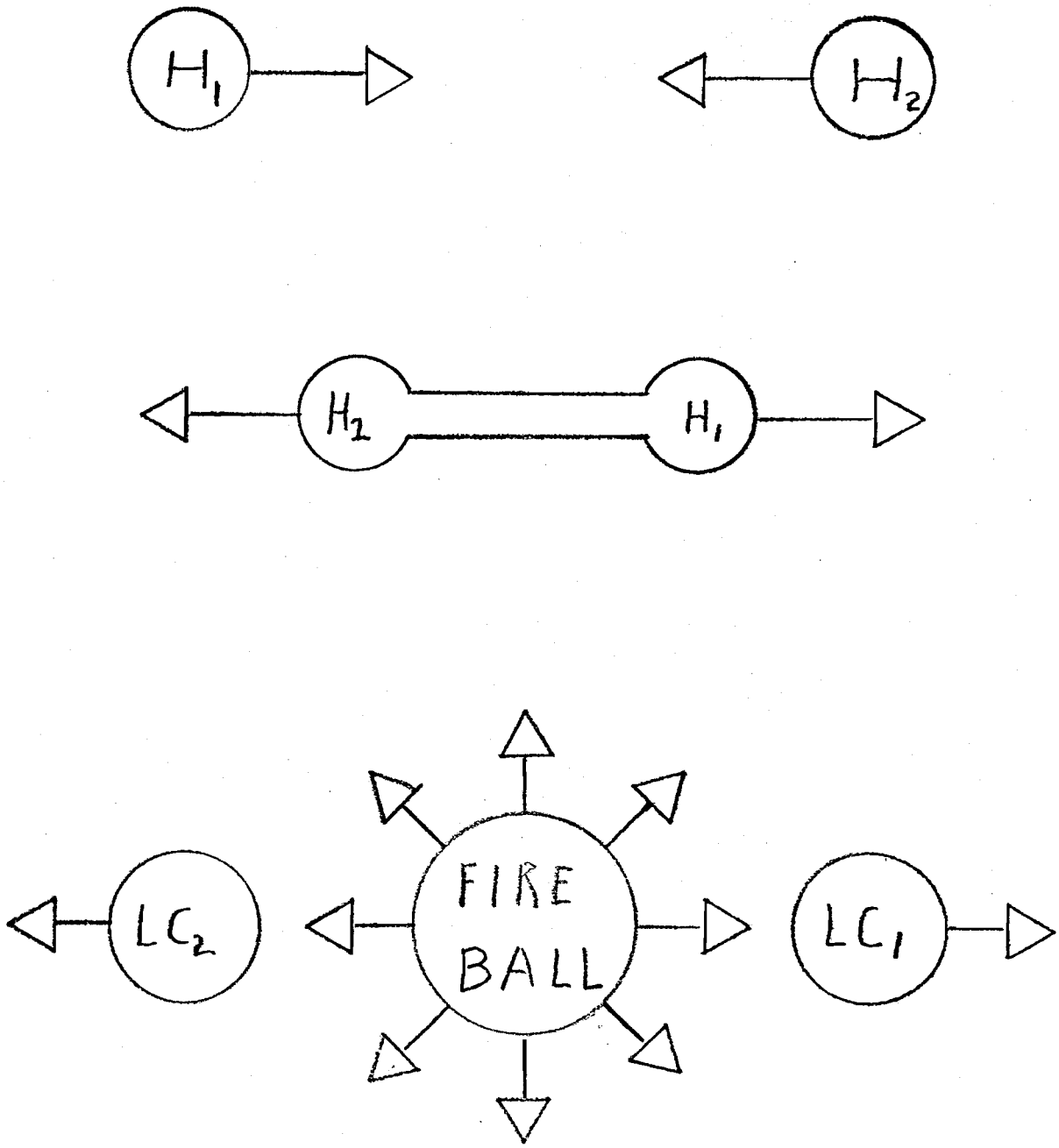

Figure 1

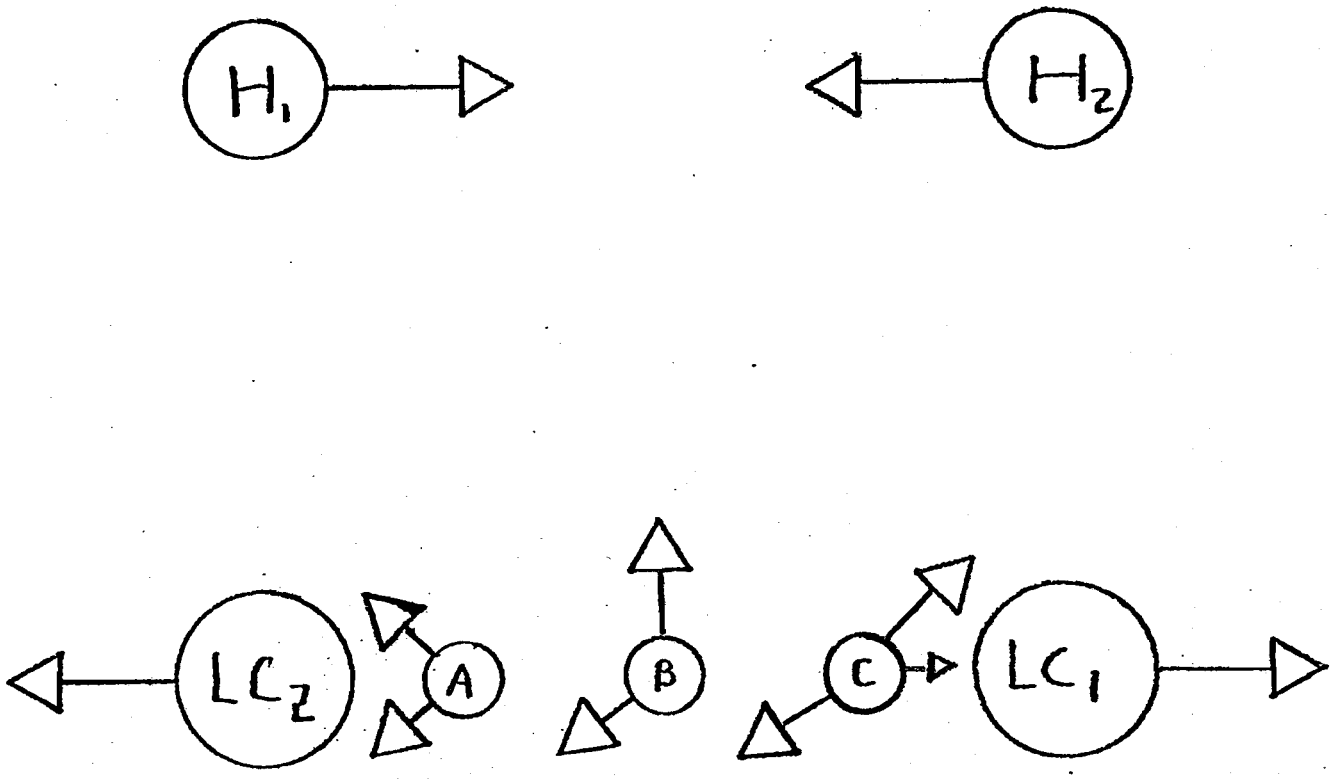

Figure 2

SCHEMATIC OF THE PROPORTIONAL
WIRE HYBRID SPECTROMETER

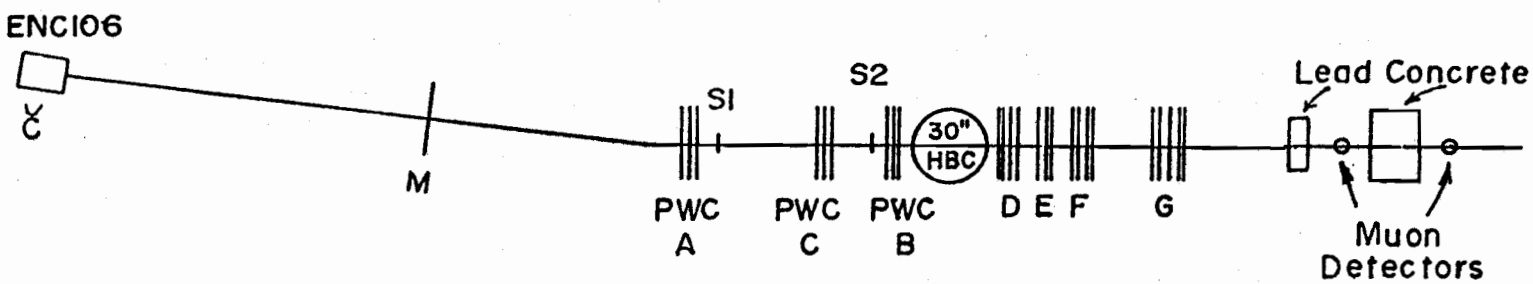

Figure 3

"INCLUSIVE AND SEMI-INCLUSIVE CHARGE STRUCTURE IN $\pi^- p$ MULTIPARTICLE PRODUCTION AT 147 GEV/c"

BROWN: D. BRICK, A.M. SHAPIRO, M. WIDGOFF

MIT: F. BARREIRO, O. BENARY, J.E. BRAU, R.I. HULSIZER, V. KISTIAKOWSKY, A. NAPIER, S. OH, I.A. PLESS, J.P. SILVERMAN

NIJMEGEN: W. KITTEL, M. SCHOUTEN

ORNL: H.O. COHN

RUTGERS: P. JACQUES, T.L. WATTS

STEVENS: E.B. BRUCKER, E.L. KOLLER, P. STAMER

TENNESSEE: W.M. BUGG, T. HANDLER

Figure 4

Figure 5

THE CONSTRUCTION OF A ZONE GRAPH

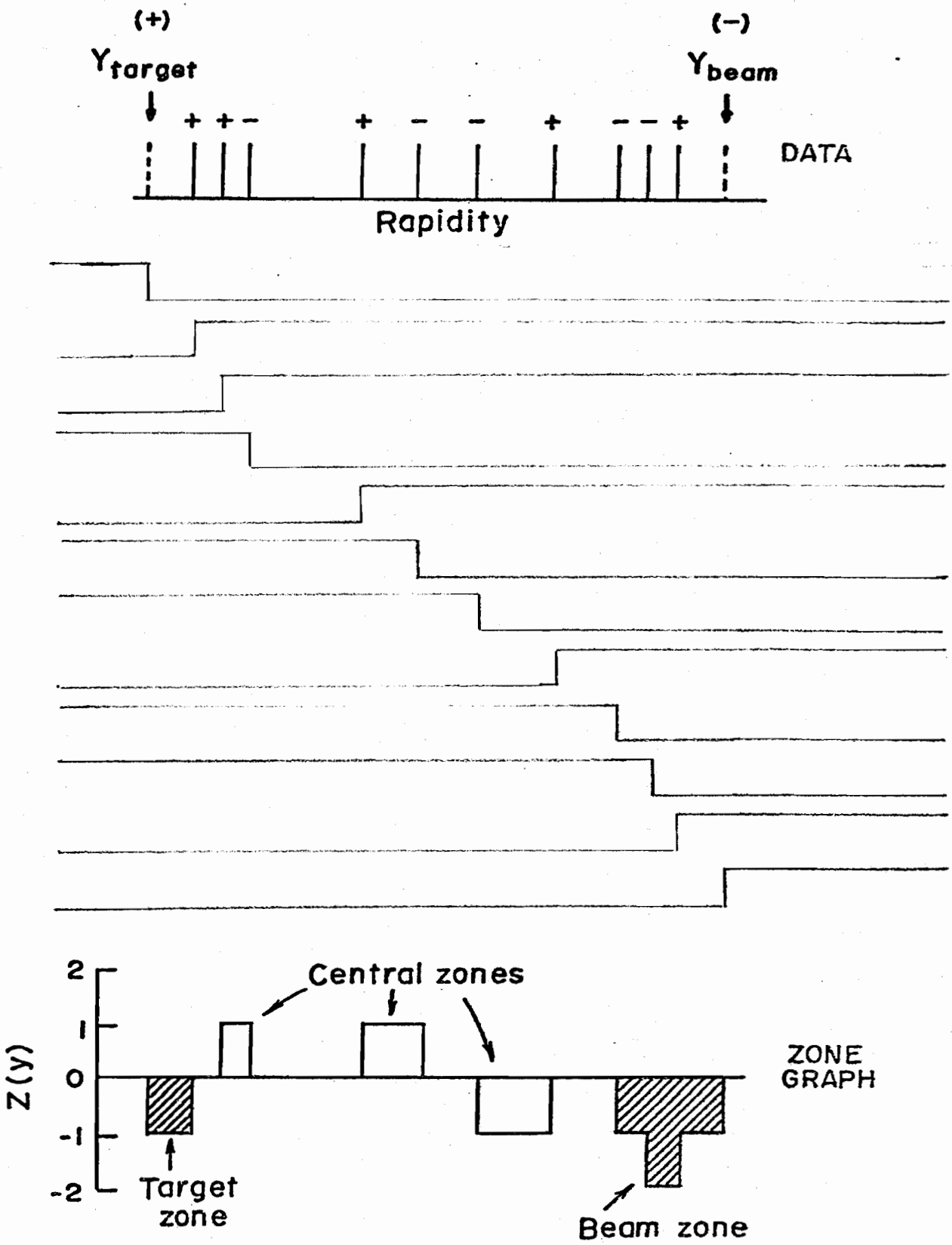

CHARGE ASYMMETRY IN RAPIDITY

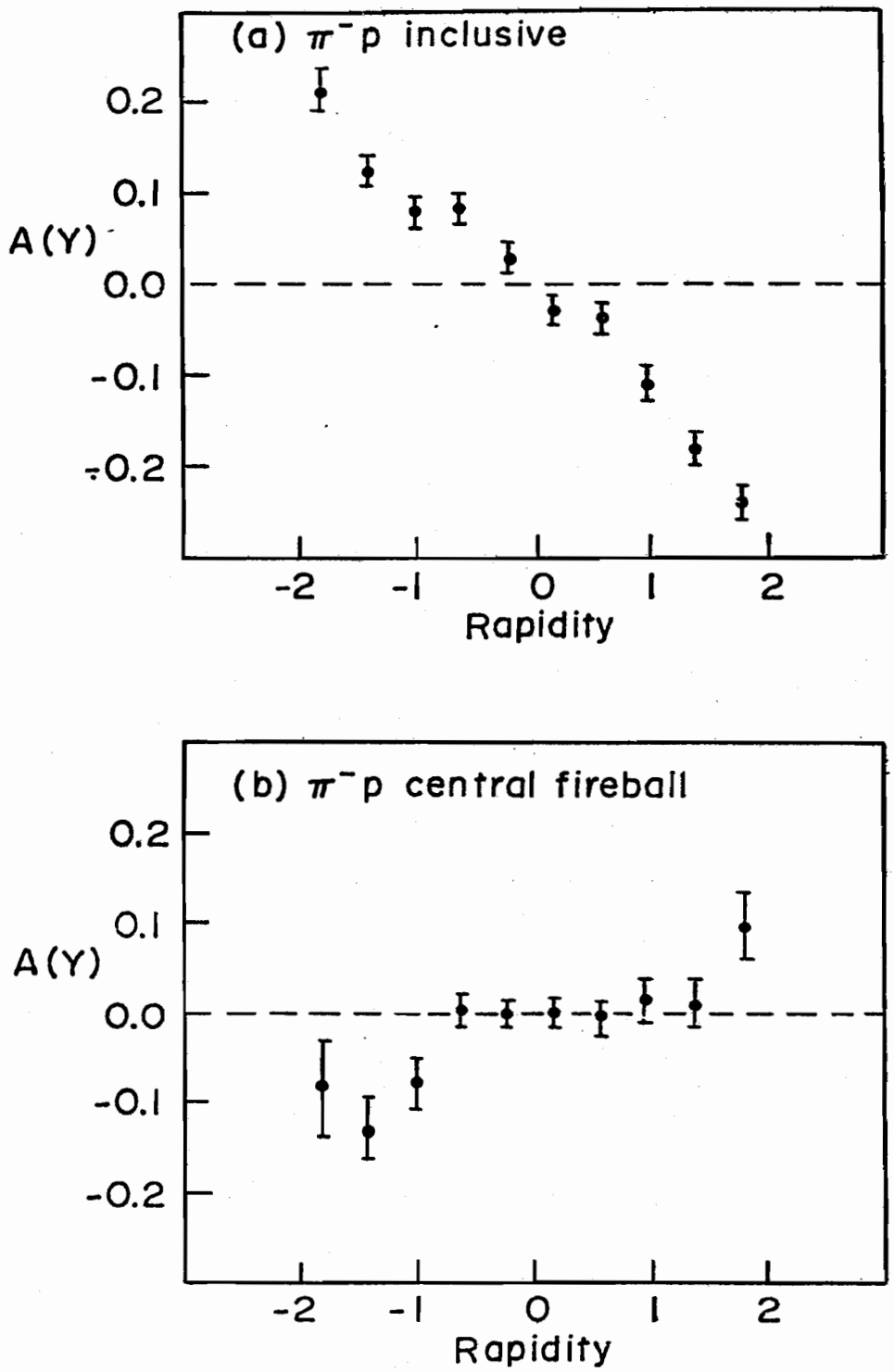

Figure 6

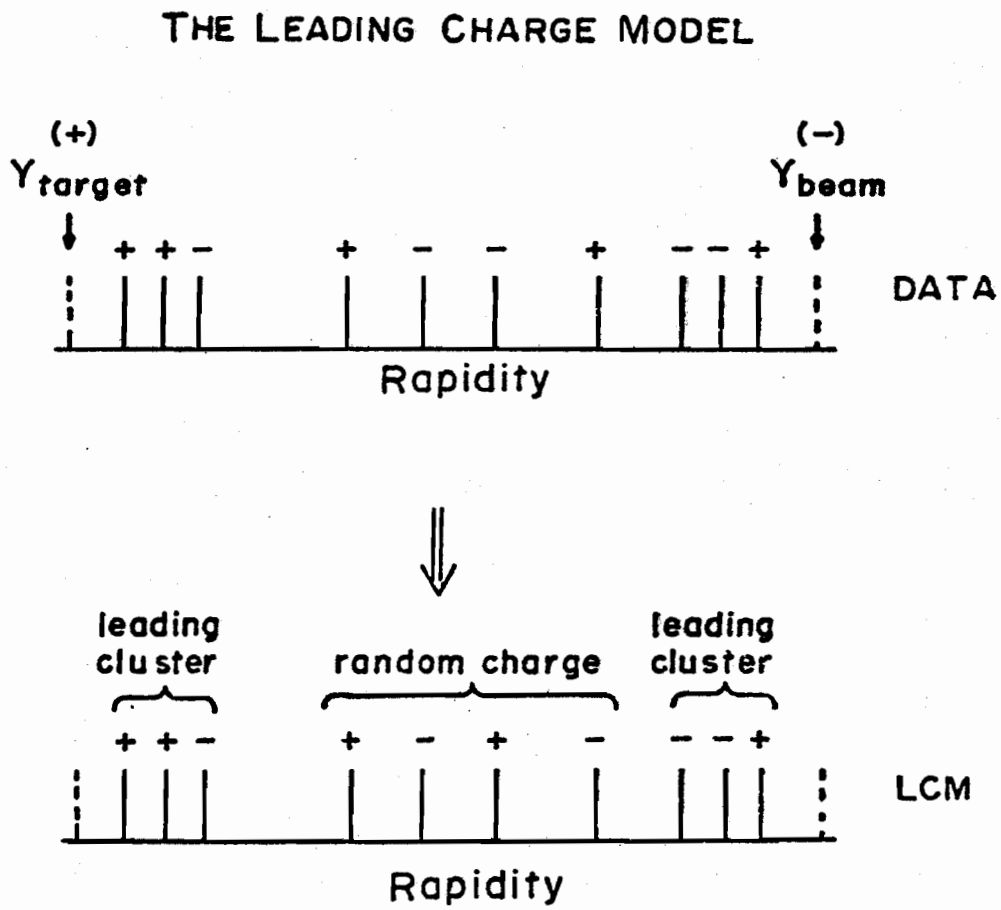
THE LEADING CHARGE MODEL
(+)
Y_{target}
(−)
Y_{beam}
+ + − + − − + − − +
DATA
Rapidity
leading cluster
random charge
leading cluster
+ + − + − + − − − +
LCM
Rapidity

Figure 7

Figure 8

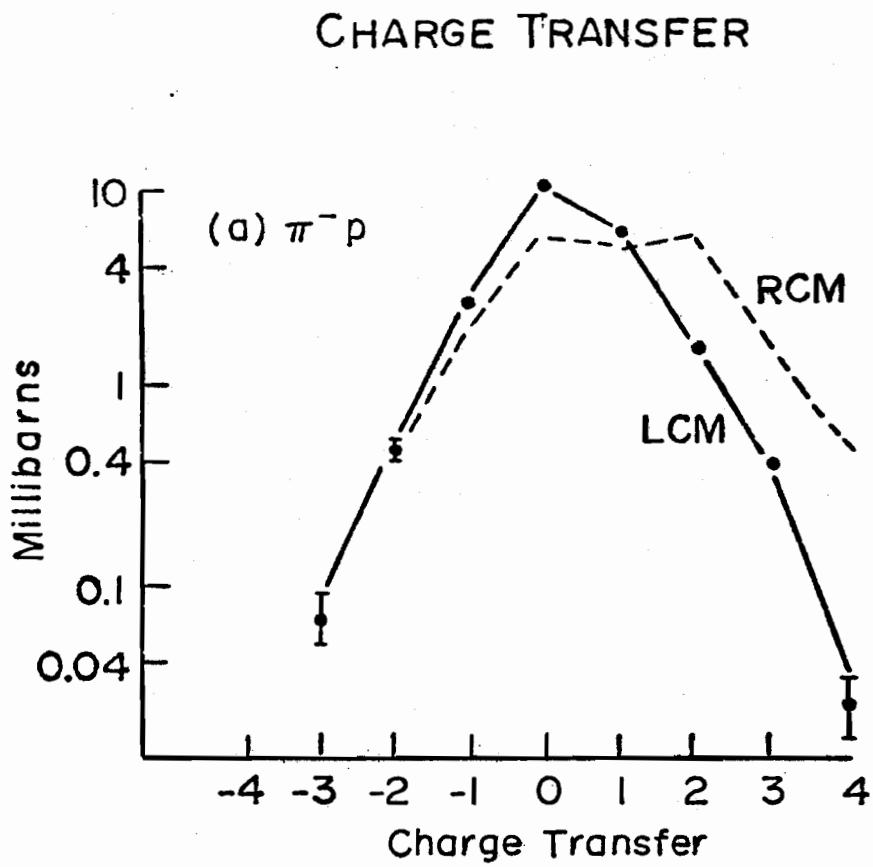
CHARGE TRANSFER
(a) $\pi^- p$
RCM
LCM
Millibarns
10
4
1
0.4
0.1
0.04
-4 -3 -2 -1 0 1 2 3 4
Charge Transfer

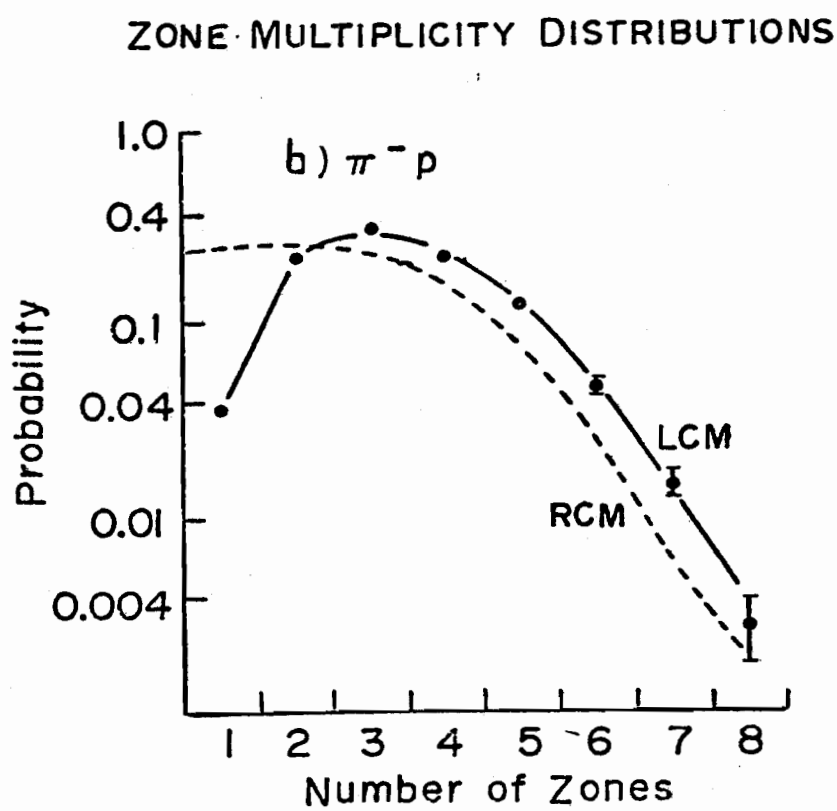
ZONE MULTIPLICITY DISTRIBUTIONS
b) $\pi^- p$
LCM
RCM
Probability
1.0
0.4
0.1
0.04
0.01
0.004
1 2 3 4 5 6 7 8
Number of Zones

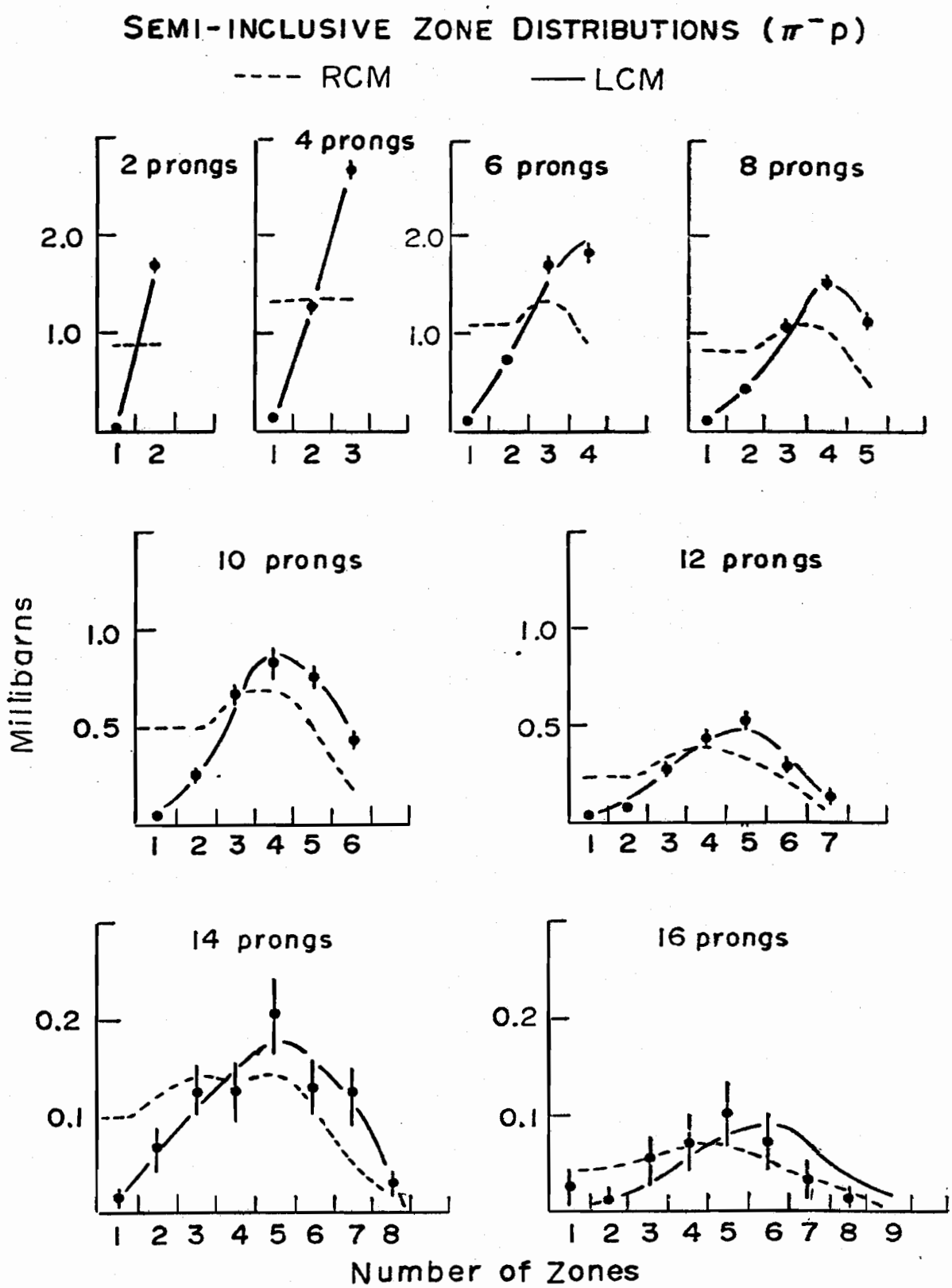
SEMI-INCLUSIVE ZONE DISTRIBUTIONS ($\pi^- p$)
---- RCM
—— LCM
2 prongs
4 prongs
6 prongs
8 prongs
10 prongs
12 prongs
14 prongs
16 prongs
Millibarns
Number of Zones

Figure 9

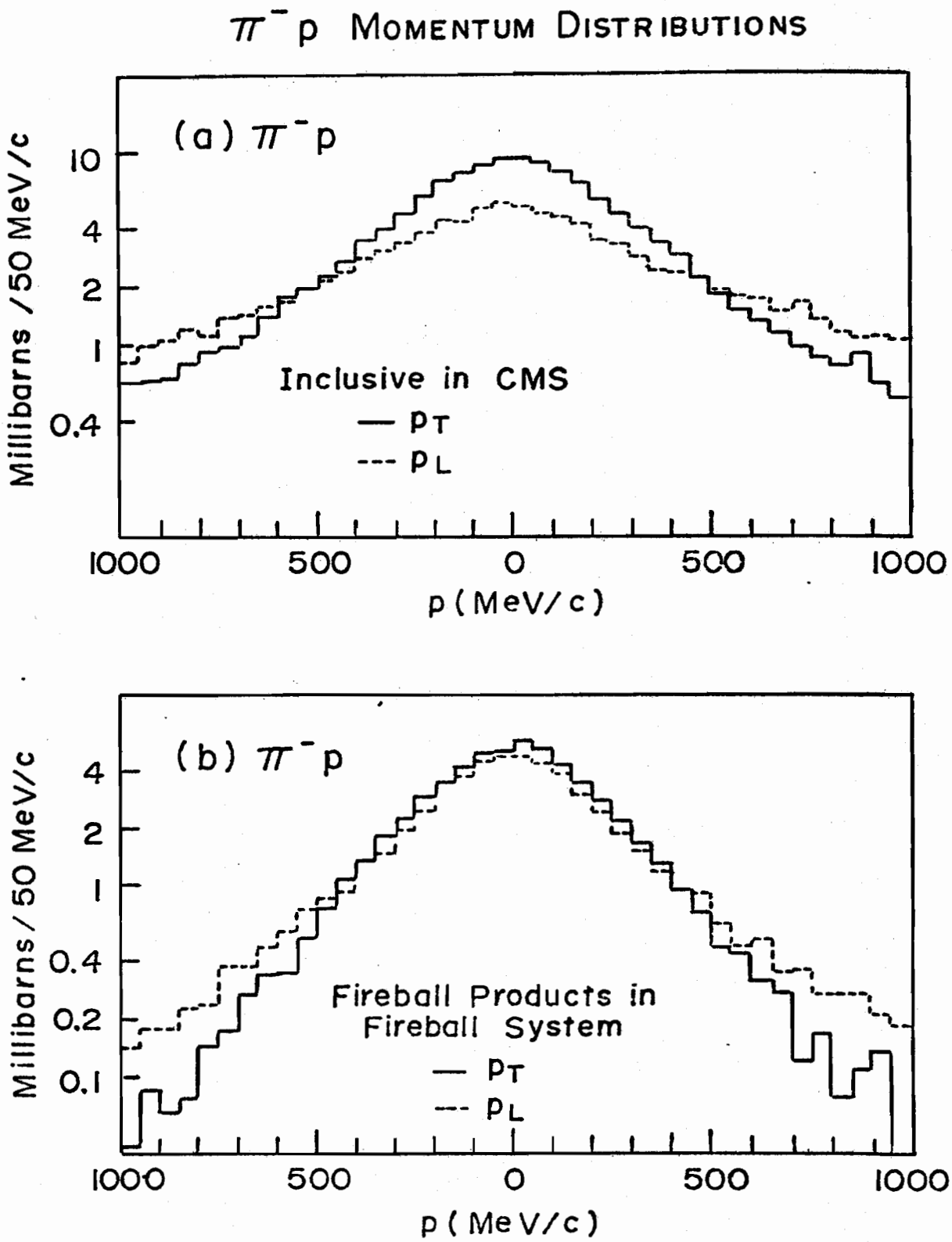
π⁻p MOMENTUM DISTRIBUTIONS
(a) π⁻p
Millibarns /50 MeV/c
10
4
2
1
0.4
Inclusive in CMS
— pT
--- pL
1000
500
0
500
1000
p (MeV/c)
(b) π⁻p
Millibarns / 50 MeV/c
4
2
1
0.4
0.2
0.1
Fireball Products in
Fireball System
— pT
--- pL
1000
500
0
500
1000
p (MeV/c)

Figure 10

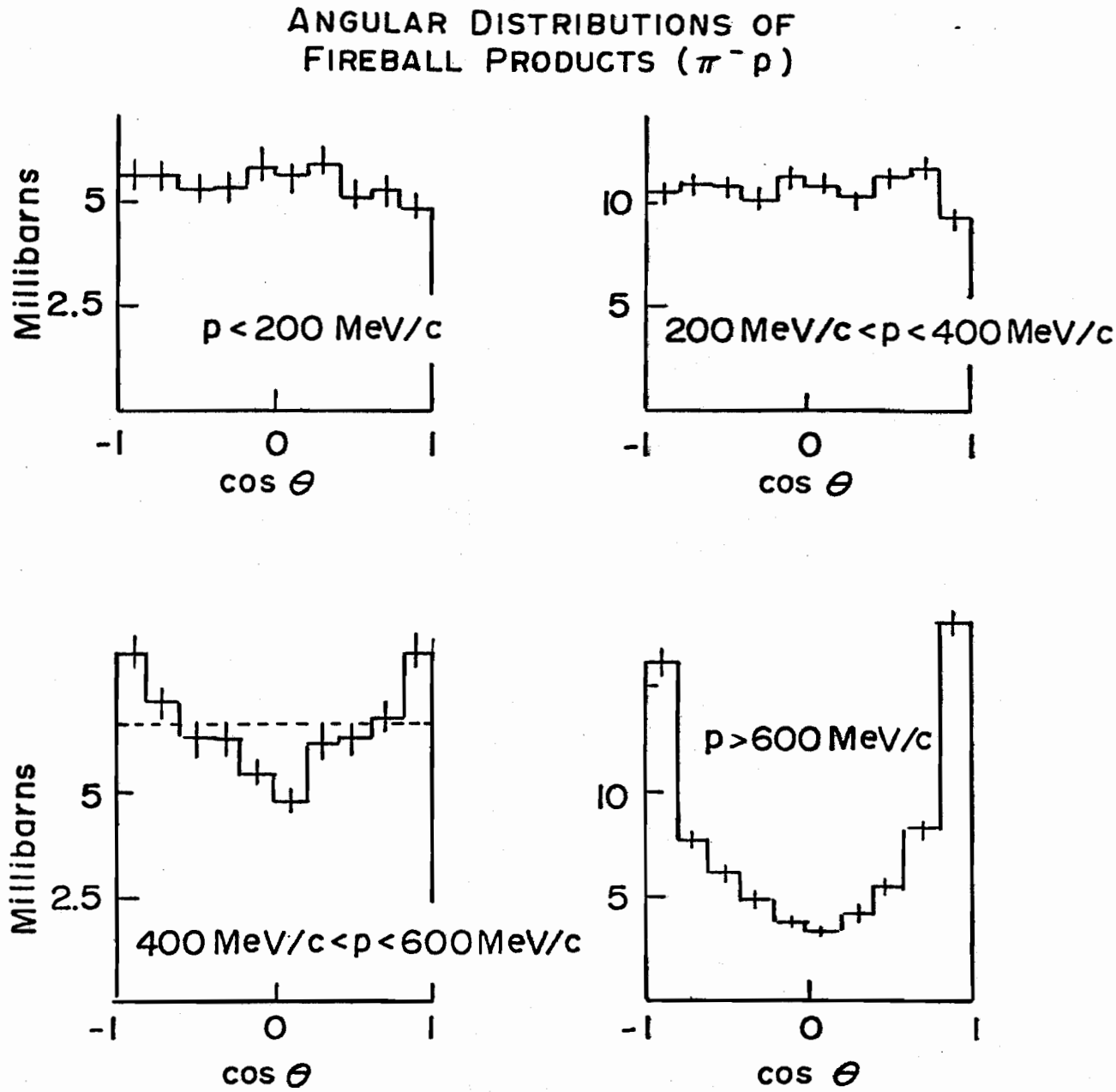
ANGULAR DISTRIBUTIONS OF
FIREBALL PRODUCTS ($\pi^- p$)
Millibarns
5
2.5
p < 200 MeV/c
-1
0
1
cos θ
10
5
200 MeV/c < p < 400 MeV/c
-1
0
1
cos θ
Millibarns
5
2.5
400 MeV/c < p < 600 MeV/c
-1
0
1
cos θ
p > 600 MeV/c
10
5
-1
0
1
cos θ

Figure 11

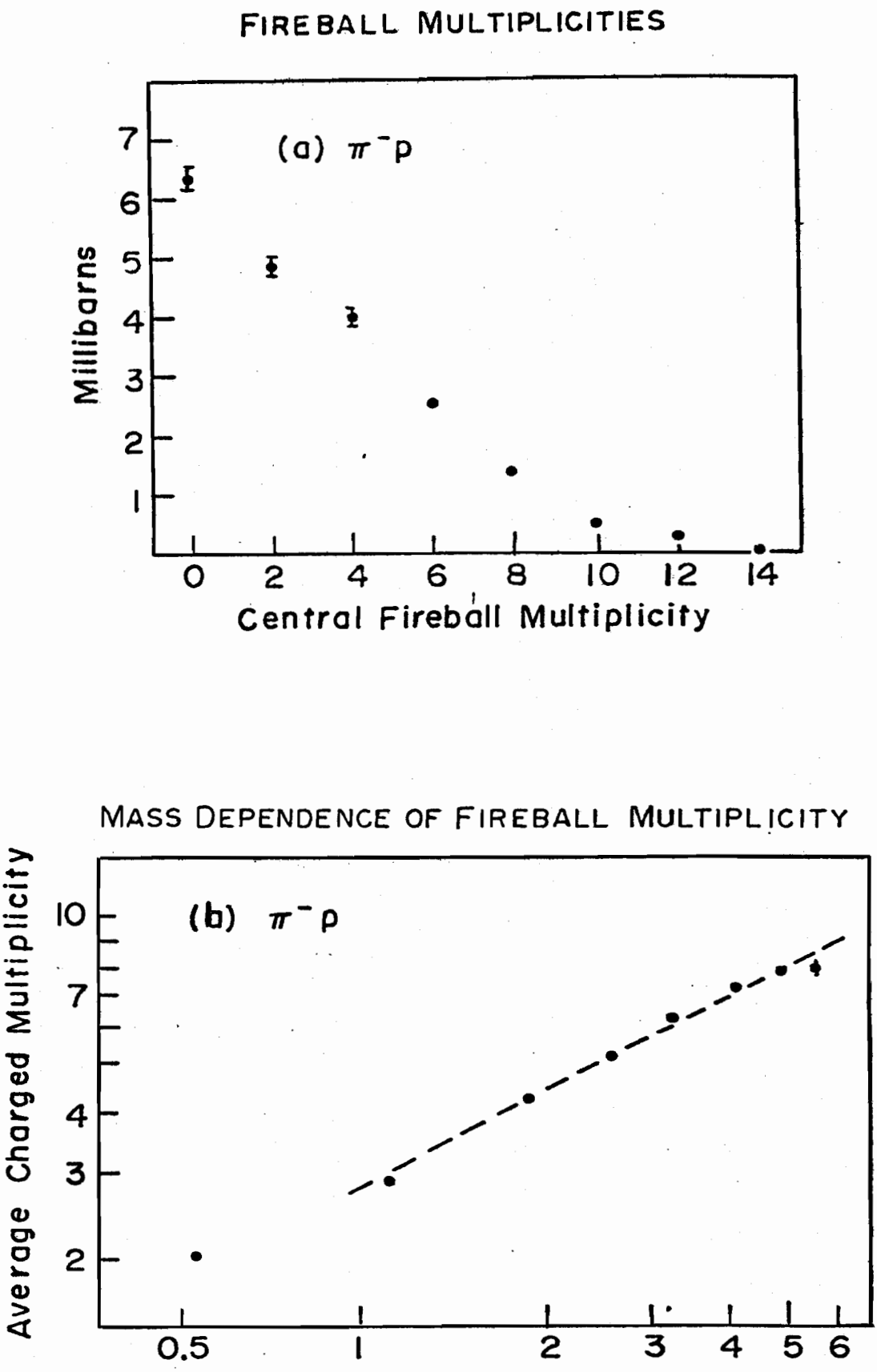
FIREBALL MULTIPLICITIES
(a) $\pi^- p$
Millibarns
7
6
5
4
3
2
1
0
2
4
6
8
10
12
14
Central Fireball Multiplicity
MASS DEPENDENCE OF FIREBALL MULTIPLICITY
(b) $\pi^- p$
Average Charged Multiplicity
10
7
4
3
2
0.5
1
2
3
4
5
6

Figure 12

FIREBALL MOMENTUM DISTRIBUTION

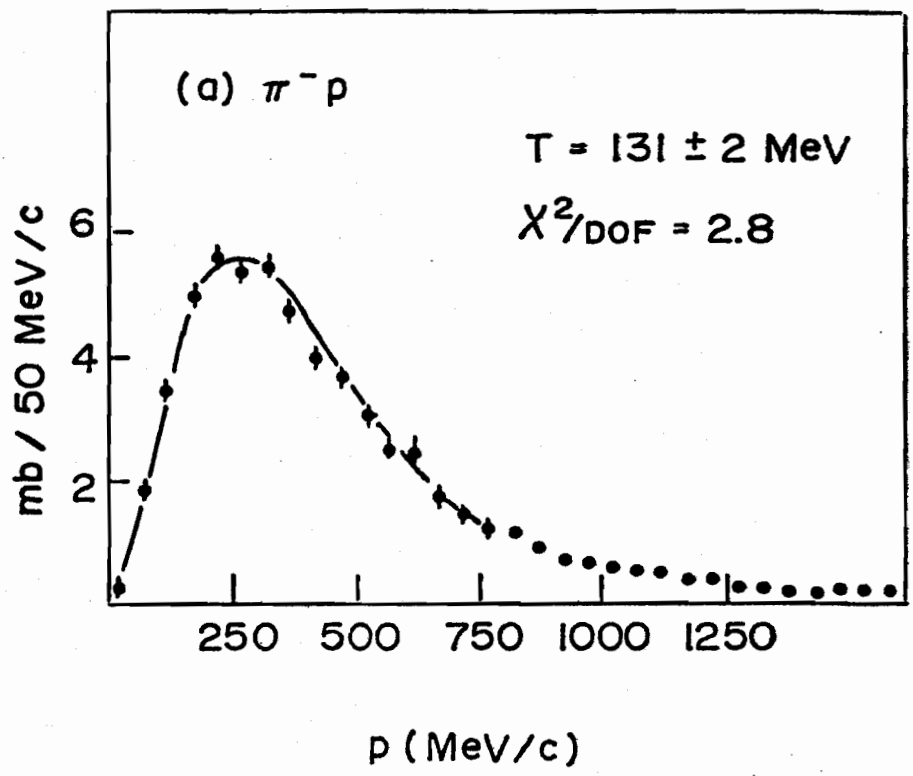

Figure 13

"MOMENTUM-SPACE STRUCTURE OF MULTI-HADRON EVENTS PRODUCED BY $\pi^- p$ INTERACTIONS AT 147 GEV/c"

BROWN: D. BRICK, A. SHAPIRO
M. WIDGOFF

IIT: H. RUBIN

INDIANA: E.D. ALYEA

MIT: E.S. HAFEN, S. OH, I.A. PLESS
R.K. YAMAMOTO

RUTGERS: T.C. OU, R.J. PLANO,
P. STAMER, T.L. WATTS

YALE: T. LUDLAM, D. LJUNG
H. TAFT

Figure 14

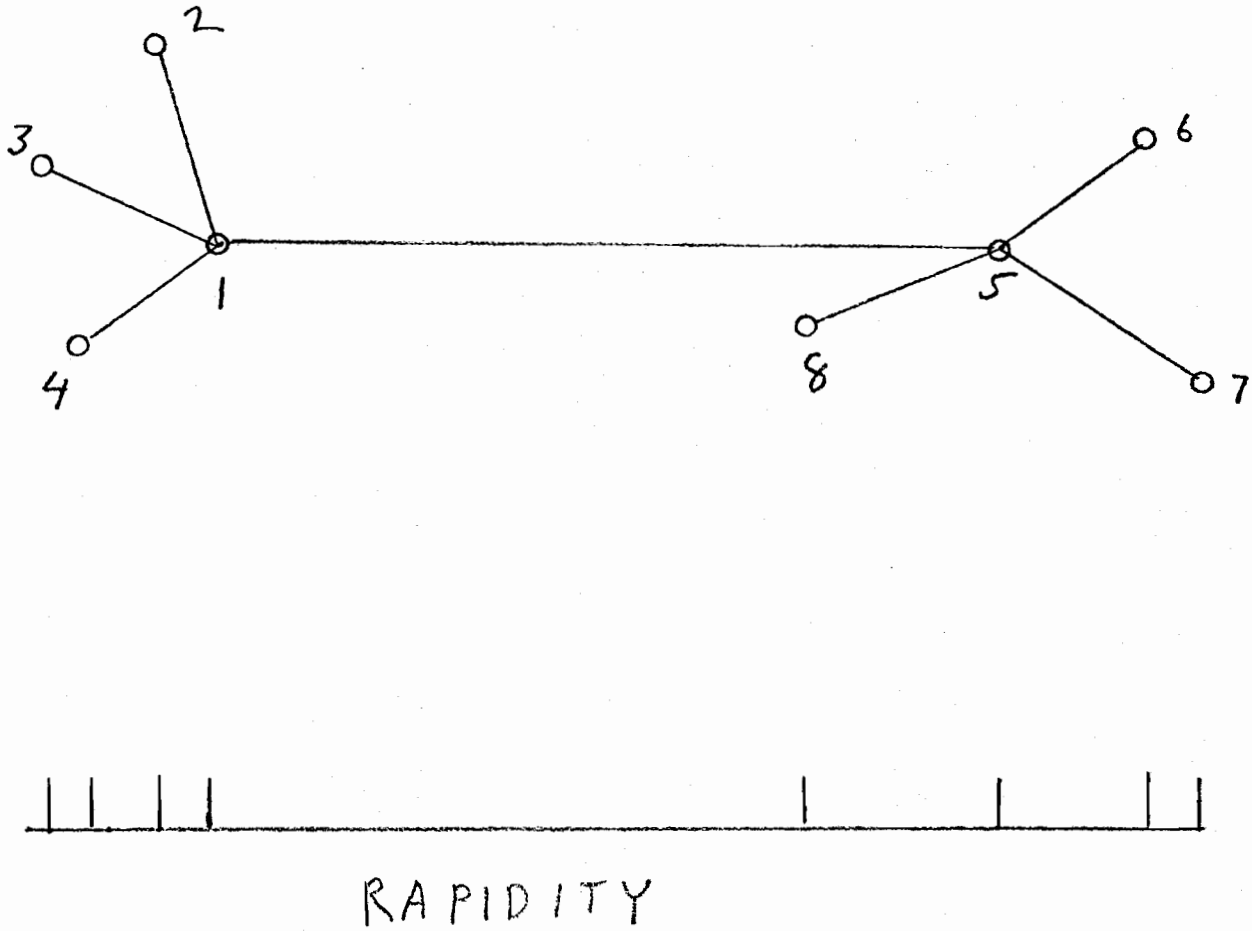

Figure 15

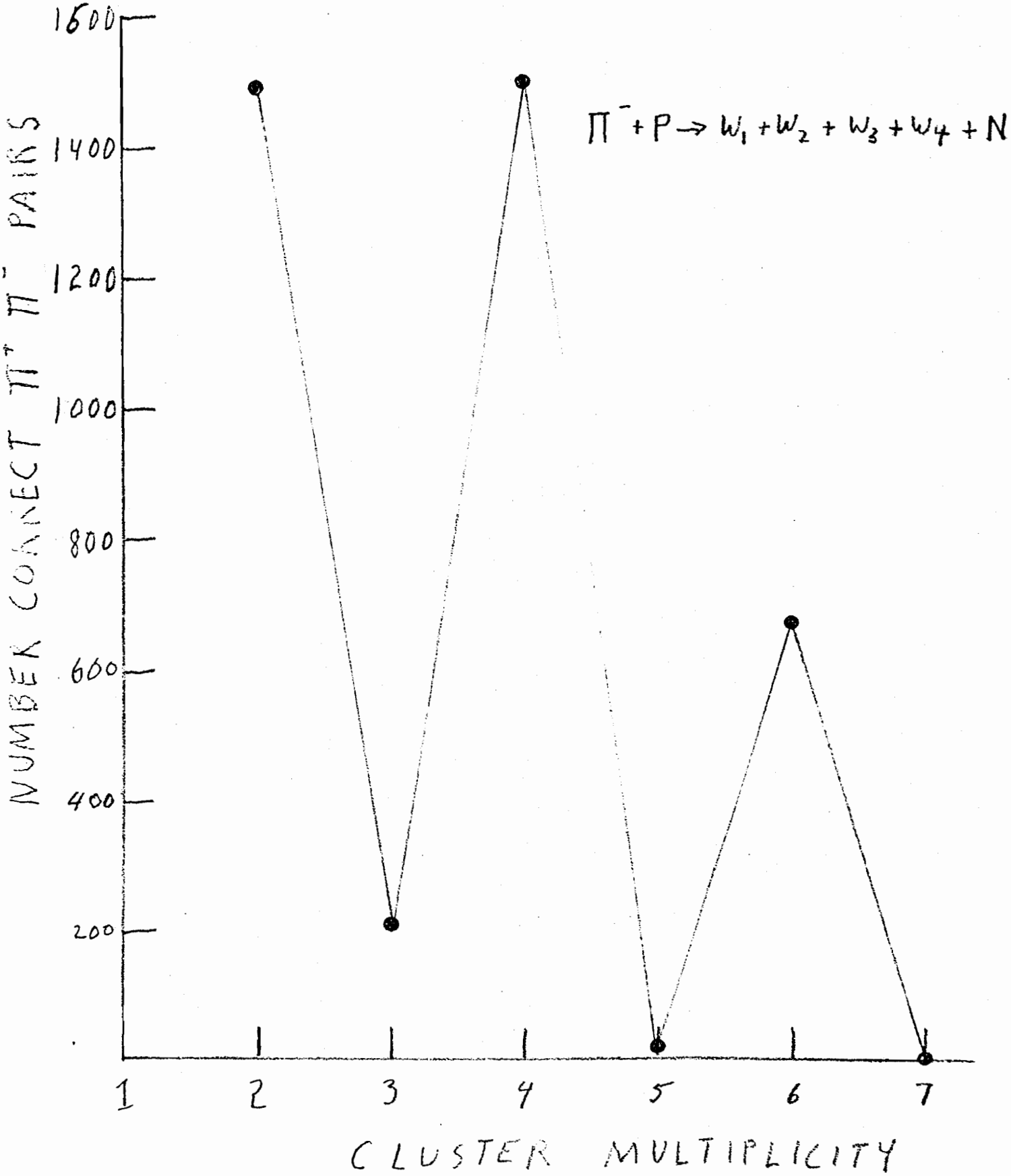
1600
1400
1200
1000
800
600
400
200
NUMBER CONNECT $\pi^+ \pi^-$ PAIRS
$\pi^- + P \rightarrow W_1 + W_2 + W_3 + W_4 + N$
1
2
3
4
5
6
7
CLUSTER MULTIPLICITY

Figure 16

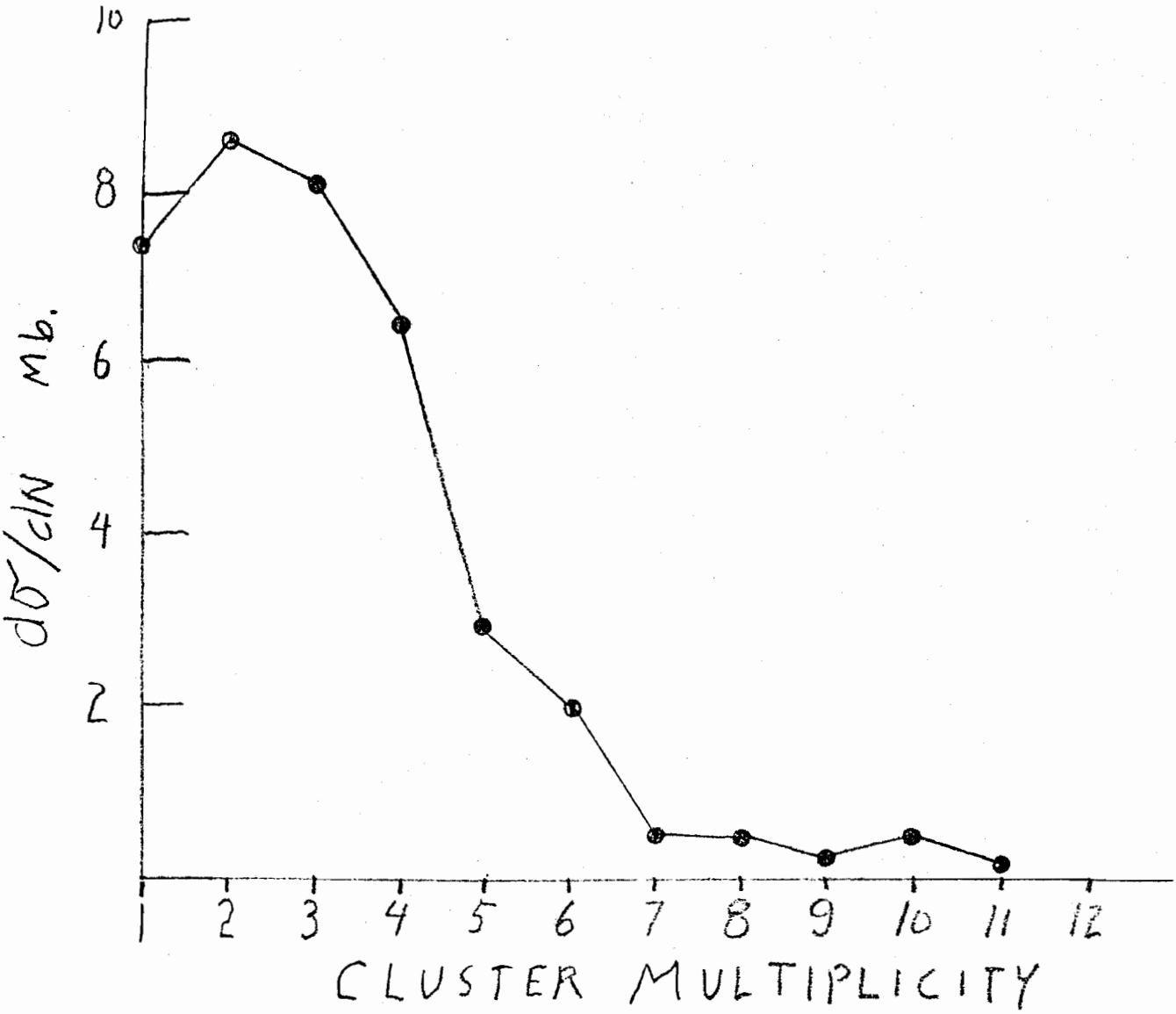

Figure 17

Figure 18

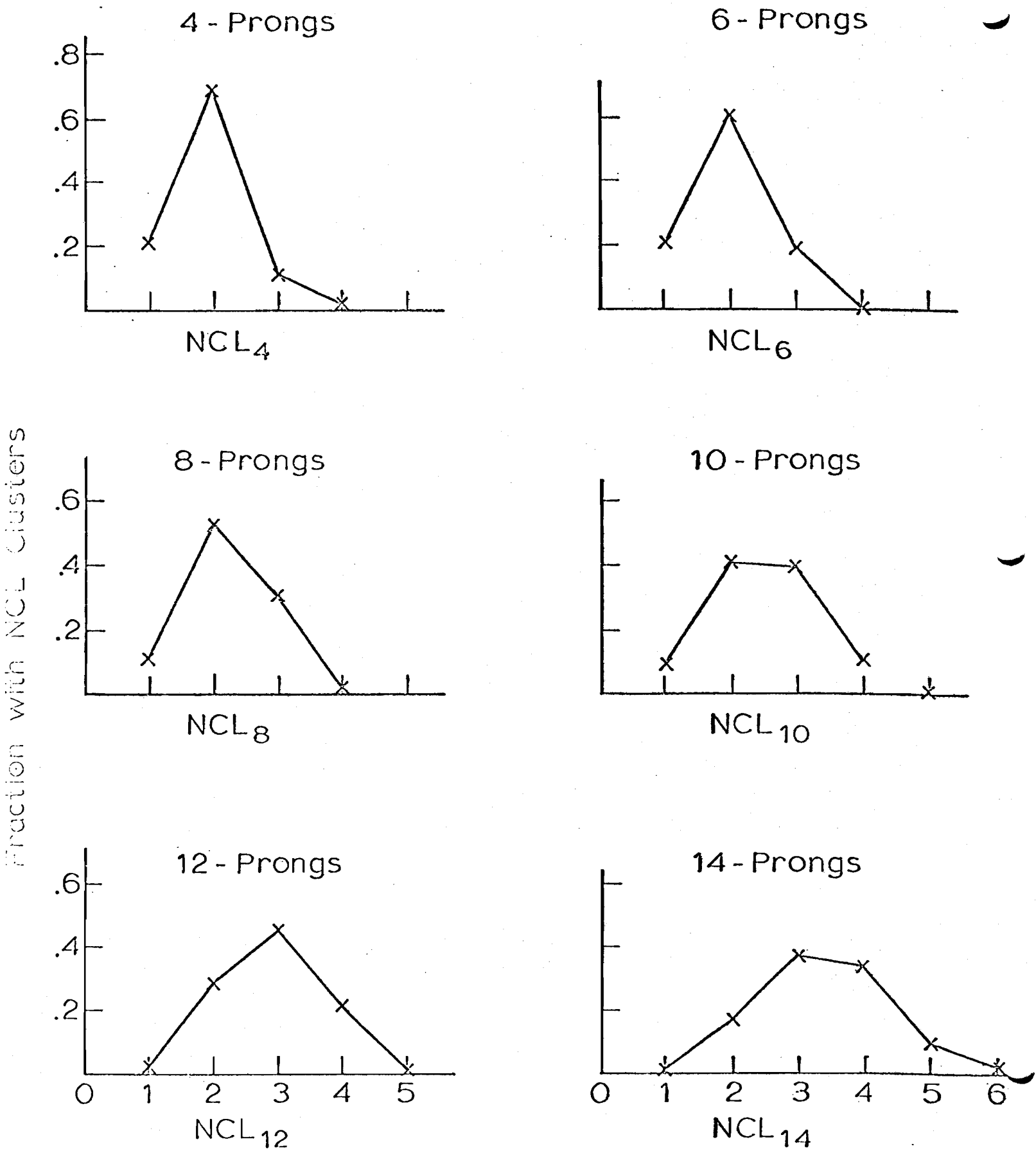
4 - Prongs
.8
.6
.4
.2
NCL4
6 - Prongs
NCL6
8 - Prongs
.6
.4
.2
NCL8
10 - Prongs
NCL10
12 - Prongs
.6
.4
.2
0 1 2 3 4 5
NCL12
14 - Prongs
0 1 2 3 4 5 6
NCL14
Fraction with NCL Clusters

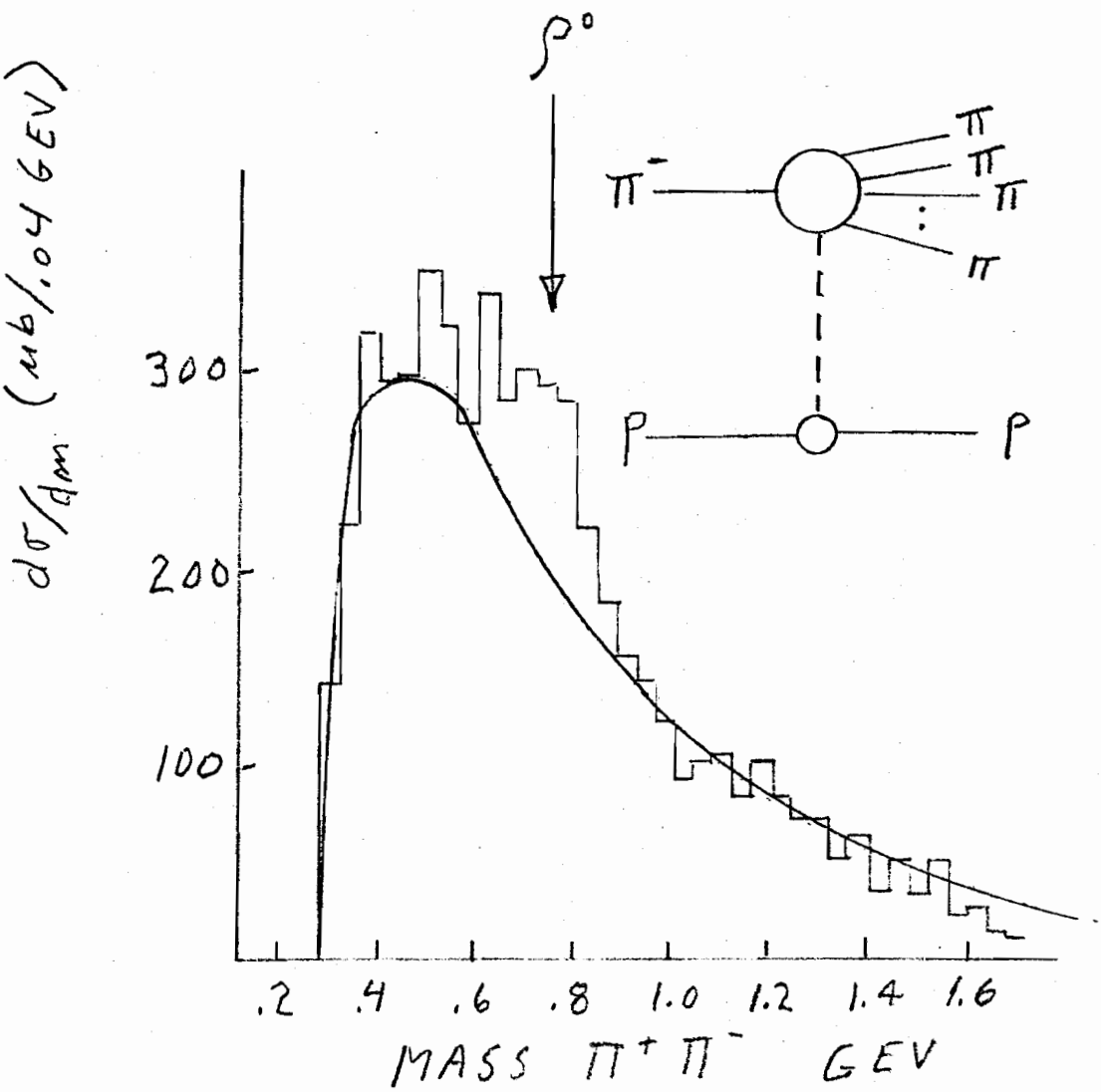

Figure 19

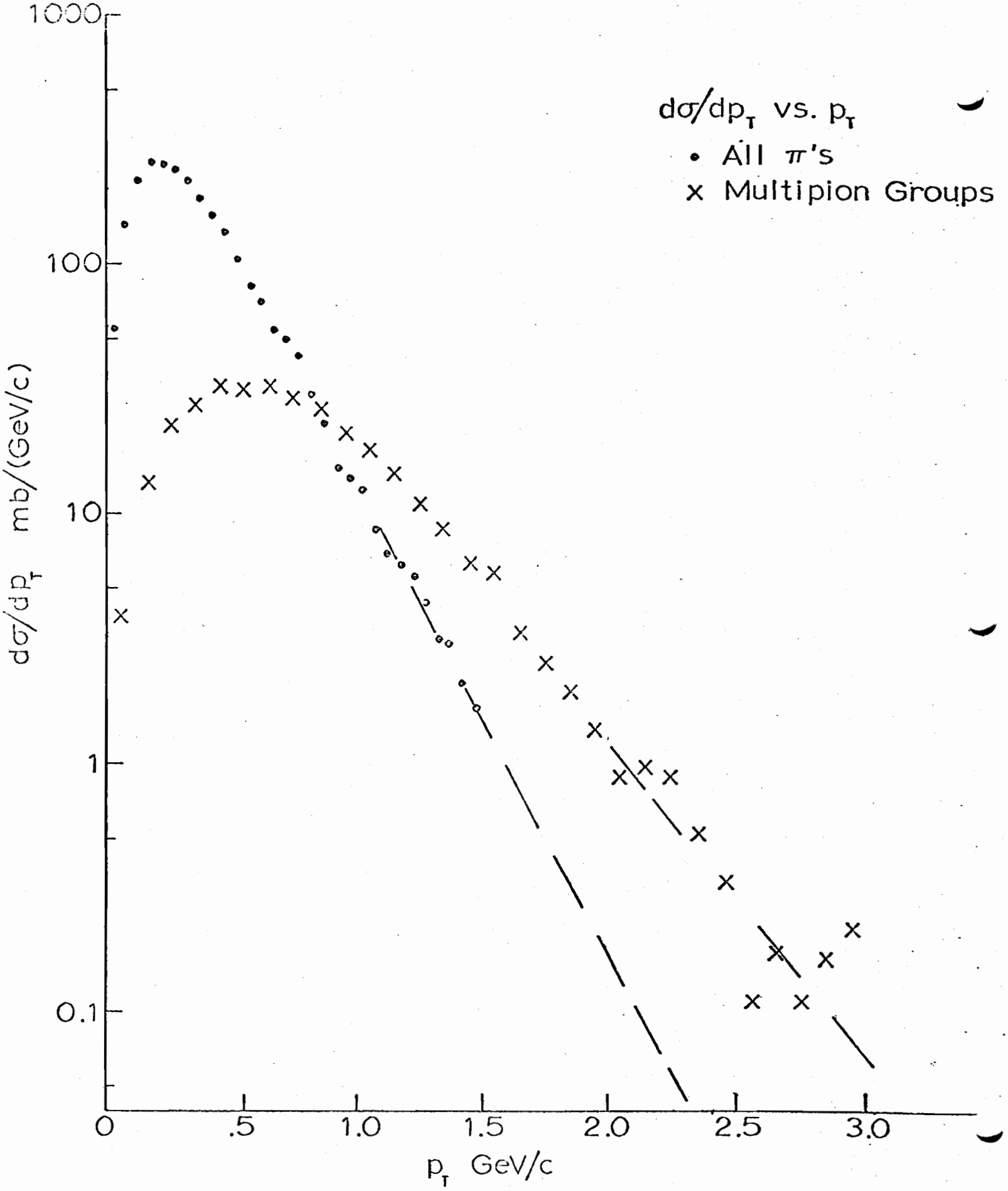
dσ/dp_T vs. p_T
• All π's
x Multipion Groups
1000
100
10
1
0.1
dσ/dp_T mb/(GeV/c)
0
.5
1.0
1.5
2.0
2.5
3.0
p_T GeV/c

Figure 20

Figure 21

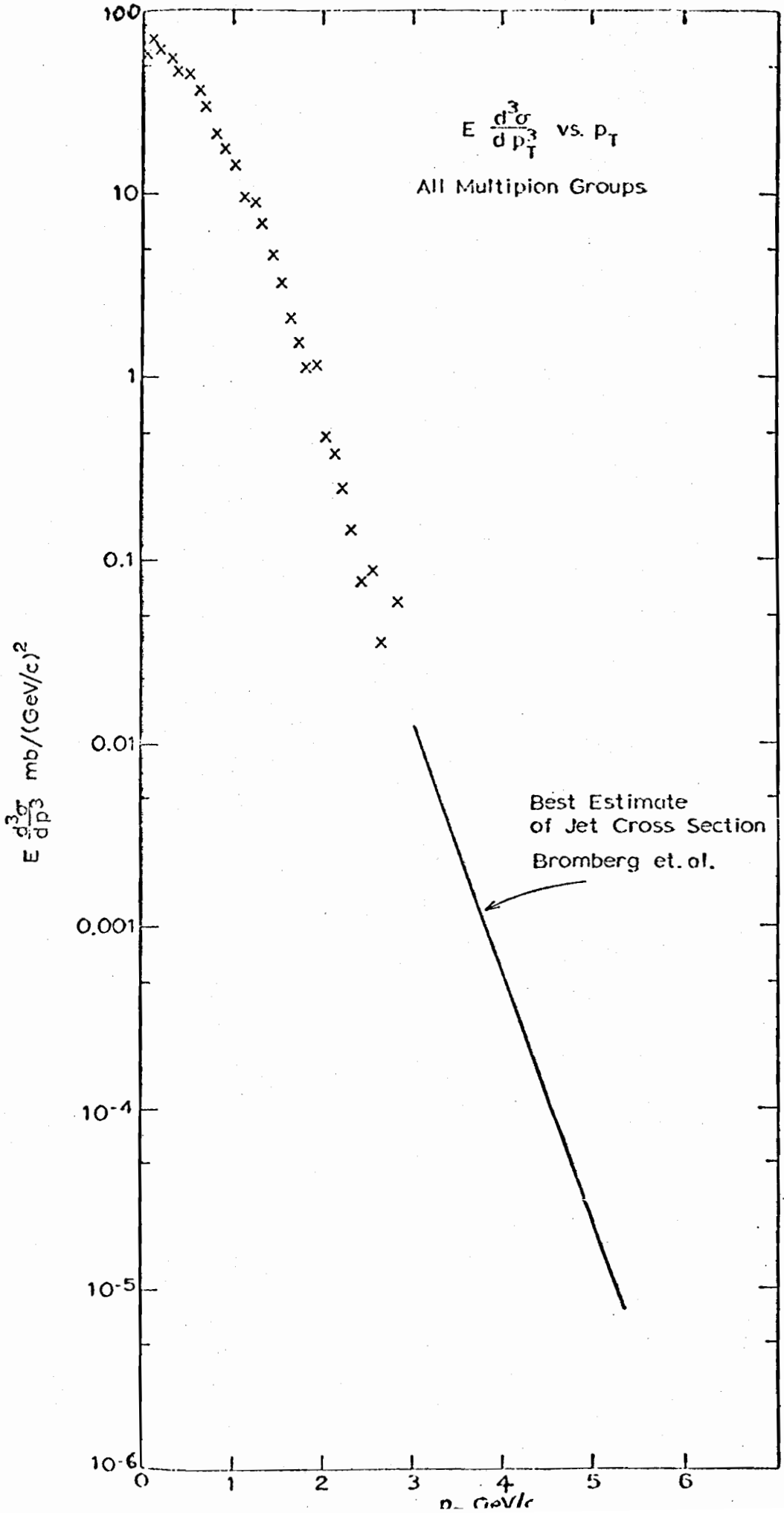
$E \frac{d^3\sigma}{dp_T^3}$ vs. p_T
All Multipion Groups
Best Estimate
of Jet Cross Section
Bromberg et. al.
$E \frac{d^3\sigma}{dp^3}$ mb/(GeV/c)^2
100
10
1
0.1
0.01
0.001
10^{-4}
10^{-5}
10^{-6}
0
1
2
3
4
5
6
p_T GeV/c